



Analytical investigation of exergetic performance on jet impingement solar air heater with multiple arc protrusion obstacles

M. M. Matheswaran¹ · T. V. Arjunan² · D. Somasundaram¹

Received: 25 May 2018 / Accepted: 13 November 2018 / Published online: 20 November 2018
© Akadémiai Kiadó, Budapest, Hungary 2018

Abstract

In this present work, an exergetic efficiency of the solar air heater (SAH) with jet impingement on multiple arc protrusion roughened absorber plate is analytically studied. It is examined out for roughness parameters of relative width ratio (W_p/W_{AP}) of 1–5, relative height ratio (e_p/d_p) of 0.5–2, relative pitch ratio (P_p/e_p) of 8–12 and angle of arc (α_a) of 35°–75°. Performance of SAH based on the second law has been effectively assessed by enumerating the useful exergy gain, irreversibility and losses occurred due to the inefficiency of the system components. Results indicate that the exergetic efficiency has been enhanced by 56.8%. Effects of roughness parameters on exergetic efficiency have been presented based on Reynolds number and temperature rise parameter. The optimized values of roughness parameters are identified, and the maximum exergetic efficiency is found to be 10.5%. Maximum exergetic destruction caused due to temperature difference between absorber plate and Sun is 65.2% at optimized conditions. In order to identify the optimum values of roughness parameters to attain the required temperature rise with maximum exergetic efficiency, design plots have been developed.

Keywords Solar air heater · Jet impingement · Exergy · Heat transfer · Artificial roughness

List of symbols

A_c	Area of absorber plate (m^2)	h_w	Convective heat transfer coefficient due to wind ($W m^{-2} K^{-1}$)
C_p	Specific heat of air ($J kg^{-1} K^{-1}$)	I	Solar radiation ($W m^{-2}$)
D	Hydraulic diameter of air flow path, m	K_i	Thermal conductivity of insulation ($W m^{-1} K^{-1}$)
d_p	Protrusion rib depth	k	Thermal conductivity of air ($W m^{-1} K^{-1}$)
e_p/d_p	Relative height ratio	L	Length of the duct (m)
e_p	Protrusion rib height	L_i	Thickness of insulation (m)
EX	Exergy (W)	m	Mass flow rate ($kg s^{-1}$)
F_R	Heat removal factor	N	Number of glass cover
F_p	Collector efficiency factor	Nu	Nusselt number
f	Friction factor of duct	P_p/e_p	Relative pitch ratio
h	Convective heat transfer coefficient ($W m^{-2} K^{-1}$)	Q_u	Useful heat gain (W)
		Re	Reynolds Number
		T	Temperature (K)
		U_L	Over all loss coefficient ($W m^{-2} K^{-1}$)
		U_b	Bottom loss coefficient ($W m^{-2} K^{-1}$)
		U_t	Top loss coefficient ($W m^{-2} K^{-1}$)
		U_e	Edge loss coefficient ($W m^{-2} K^{-1}$)
		V_w	Wind velocity ($m s^{-1}$)
		W_p	Width of the collector (m)
		W_{AP}	Width of single arc rib
		W_p/W_{AP}	Relative width ratio
		X/D	Stream wise pitch ratio
		Y/D	Span wise pitch ratio

✉ M. M. Matheswaran
madhume01@gmail.com

T. V. Arjunan
arjun_nivi@yahoo.com

D. Somasundaram
soms.iitm@gmail.com

¹ Department of Mechanical Engineering, Jansons Institute of Technology, Coimbatore, Tamilnadu 641659, India

² Department of Mechanical Engineering, Coimbatore Institute of Engineering and Technology, Coimbatore, Tamilnadu 641109, India

μ	Viscosity ($\text{kg m}^{-1} \text{s}^{-1}$)
Z	Duct depth (m)
ρ	Density (kg m^{-3})
σ	Stefan Boltzmann constant ($\text{W m}^{-2} \text{K}^{-4}$)
ε	Emissivity
α	Absorptivity
α_a	Angle of arc ($^\circ$)
$\Delta T/I$	Temperature rise parameter ($\text{K m}^2 \text{W}^{-1}$)
$\alpha_a/55$	Relative angle of arc
η_I	Thermal efficiency
η_{II}	Exergetic efficiency
η_{Eff}	Thermo-hydraulic efficiency

Subscripts

o	Outlet
i	Inlet
a	Ambient
g	Glass
ap	Absorber plate

Introduction

Thermal energy conversion using solar air heater has been considered as a one of the most promising techniques that can be used for supplying a hot air for space heating, drying of agriculture and industrial products [1]. Properties of air such as low density, small volumetric heat capacity and lower thermal conductivity lead to lower heat transfer coefficient between absorbing surface and working fluid [2–4]. Consequently, it results in lower thermal efficiency of the system. To improve its performance, various configurations such as artificially roughened plate SAH with various types of roughness geometries, multi-pass flow configurations, flow combined with recycling, packed bed system have been analyzed experimentally and analytically [5–7]. Further, the researchers identified that air jet with impingement on smooth and artificially roughed plate enhances the value of heat transfer coefficient by creating more turbulence underneath the absorber plate. As a result of jet impingement, the performance of SAH was considerably improved by 21.2% [8, 9].

Jet plate design has major impact on thermal performance of SAH, the detailed investigation of its parameters is discussed in the literature. Chauhan and Thakur [10] studied the effect of jet plate design parameters on impinging jet solar air heater with smooth plate and concluded that there was enhancement in 2.67 times of heat transfer and 3.5 times of friction factor when compared it with conventional parallel pass SAH. They also evaluated the thermo-hydraulic performance for the identical configuration of SAH and reported that the maximum effective

efficiency was 70% [11]. The performance of jet impingement SAH depends on channel spacing between absorber and jet plate and jet diameter ratio of 0.07 gives maximum thermal performance with cross flow condition [12, 13]. Further, SAH performance is improved by parallel pass jet impingement technique and concluded the maximum energy and exergy efficiency ratio is improved by 2.15 and 3.4 times at Bangalore climatic conditions [14]. Further, micro-jet impingement SAH is developed and its thermal efficiency ranges from 66 to 90% at laboratory testing conditions [15].

Even though the experiments and analytical studies provide performance of SAH, optimization is required for identifying the decisive parameters of the design. The jet plate design parameters are optimized using performance search index and Taguchi methods. It was concluded that a significant effect of stream wise pitch, span wise pitch and jet diameter on thermal performance of SAH is of 9.5%, 41.6% and 48.8%, respectively [16, 17]. A mathematical model developed for predicting the thermal efficiency of PV/T collectors with jet impingement with an accuracy of 10% when compared with experimental results [18].

Even though the thermal systems are analyzed based on energy basis, it is demonstrated that first law- and second law-based exergy analyses have been considered superior for comparison, optimization and performance evaluation. Exergy has been a useful tool to measure the maximum work potential and inefficiencies of individual components that causes the irreversibility [19–21]. The exergetic performance of the artificially roughened solar air heaters are compared by Gupta and Kaushik [22] and reported that artificial roughed designs have been suitable for air heaters with higher flow cross sectional area with lower Reynolds number.

Then, further investigations for various configurations of artificially roughened SAH are analytically analyzed and the roughness parameters are optimized to maximize the second law efficiency [23–26]. Bahrehmand et al. [27] analyzed eight different configurations of SAH based on exergetic performance and evaluated the effect of Reynolds number, channel depth and channel length. They also concluded that thin metal sheet SAH with double glass cover has better performance at lower Reynolds number ($Re < 4000$) and thin metal sheet SAH with single glass cover has highest exergetic efficiency at higher Re . The exergy-based optimum design and operating conditions have been studied for double-pass V-corrugated SAH by Hedayatzadeh et al. [28, 29] using genetic algorithm. Their analytical investigation shows that low inlet air temperatures, low area ratio and increasing number of glasses leads to higher exergetic efficiency and that the maximum exergy losses occurs at exergy destruction due to temperature difference between sun and absorber plate.

Nadda et al. [30] experimentally formulated the correlation for Nusselt number and friction factor for solar air heater with jet impingement on multiple arc shape roughness with accuracy of $\pm 9\%$ and $\pm 11\%$, respectively.

It is concluded that solar air heaters with jet impingement on smooth plate are investigated for various design and operating conditions and the results are reported in the form of thermal efficiency and thermo-hydraulic efficiency. On the other hand, artificially roughened solar air heaters are effectively designed and optimized using exergetic analysis. However, the exergetic performance optimization of solar air heaters with jet impingement on artificially roughened plates has not been investigated.

The objective of the present work is focused on analytically evaluating the exergetic performance of the solar air heater with jet impingement on multiple arc protrusion roughened absorber plate. Based on the loss-based exergetic performance evaluation, the values of surface roughness parameters such as relative width ratio (W_p/W_{AP}), relative height ratio (e_p/d_p), relative pitch ratio (P_p/e_p) and relative angle of arc (α_a) are to be optimized as a function of Reynolds number and temperature rise parameter. The design plots will be prepared in order to identify the optimum values of roughness parameters to attain the desired values of temperature rise. The results, obtained for solar air heater with jet impingement on smooth plate working at identical conditions, will also be compared with multiple arc protrusion roughened plate with jet impingement SAH.

Performance analysis of solar air heater with jet impingement

Thermal performance

The schematic diagram of the solar air heater is shown in Fig. 1a. The arrangements of roughness and their nomenclature and Jet plate configuration have been shown in Fig. 1b, c, d. The thermal performance of a solar air heater with jet impingement is calculated based on first law of thermodynamics which describes that the thermal efficiency of SAH is the ratio between instantaneous rates of useful energy gain over a time period to solar insolation incident on the surface over the same time period.

$$\eta_{th} = \frac{Q_u}{IA_c} \quad (1)$$

The thermal efficiency can also be expressed in terms of heat removal factor (F_R) [31]

$$\eta_{th} = \frac{mC_p(T_o - T_i)}{IA_c} = F_R \left[(\alpha\tau) - U_L \left(\frac{T_i - T_a}{I} \right) \right] \quad (2)$$

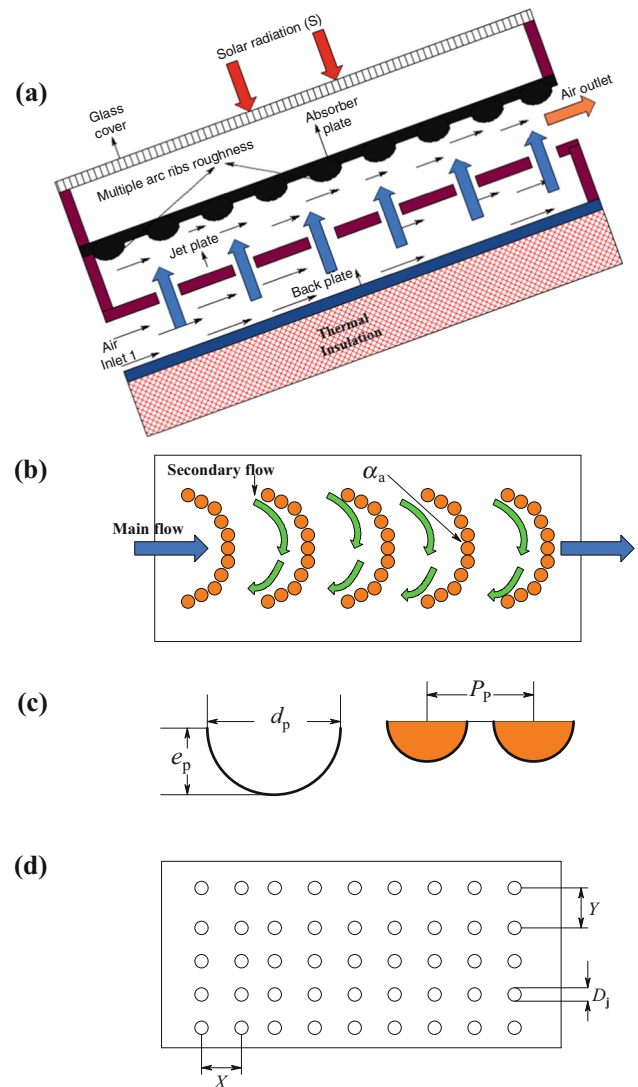


Fig. 1 a Schematic layout of SAH with jet impingement on multiple arc-shaped obstacles, b absorber plate, c detailed view of obstacles and d jet plate

Thermo-hydraulic performance

Thermal performance of the solar air heater is improved due to impinging of higher velocity jets on artificially roughened absorber plate. However, this augmentation of heat transfer also consumes the additional pumping power. Therefore, the thermal energy equivalent of pumping power must be subtracted from the overall heat energy gain to calculate the actual performance of SAH by the following equation [32].

$$\eta_{Eff} = \frac{Q_u}{I \times A_c} - \left[\frac{P_m}{I \times A_c \times C_j} \right] \quad (3)$$

In the above equation P_m represents the pumping power and C_j represents thermal energy conversion factor and it is

equal to 0.2 [32]. The pumping power is calculated using the relation

$$P_m = \rho_a V^3 f L(W + H) \tag{4}$$

$$\eta_{\text{Eff}} = \frac{Q_u}{I \times A_C} - \left[\frac{\rho_a V^3 f L(W + H)}{I \times A_C \times C_j} \right] \tag{5}$$

Exergy analysis

Exergy analysis of a solar air heater describes the maximum work potential that can be extracted from the energy input. It is a powerful tool for analyzing the system thermodynamically and designing an energy efficient SAH by minimizing exergy destruction or by maximum exergy delivery. By using the exergy analysis, the SAH components can effectively be optimized by considering the both useful energy gain and required pumping power. Figure 2 depicts the exergy balance for a solar air heater with jet impingement. Exergy balance for the solar air heater can be written as

$$\Sigma EX_{\text{in}} - \Sigma EX_{\text{out}} = \Sigma EX_{\text{losses}} \tag{6}$$

The above equation can be re written as follows:

$$EX_{\text{heat}} - EX_{\text{Work}} + EX_{\text{massin}} - EX_{\text{massout}} = EX_{\text{losses}} \tag{7}$$

Equation 7 can be expressed in general form of exergy balance is written as:

$$IA_c \left[1 - \frac{4}{3} \left(\frac{T_a}{T_{\text{sun}}} \right) + \frac{1}{3} \left(\frac{T_a}{T_{\text{sun}}} \right)^4 \right] - \dot{m}(h_{\text{out}} - h_{\text{in}}) - T_a(S_{\text{out}} - S_{\text{in}}) = EX_{\text{losses}} \tag{8}$$

Further, the enthalpy and entropy terms in Eq. 8 is stated as follows:

$$IA_c \left[1 - \frac{4}{3} \left(\frac{T_a}{T_{\text{sun}}} \right) + \frac{1}{3} \left(\frac{T_a}{T_{\text{sun}}} \right)^4 \right] - \dot{m}C_p(T_{\text{out}} - T_{\text{in}}) + \dot{m}C_p T_a \ln \left[\frac{T_{\text{out}}}{T_{\text{in}}} \right] - \dot{m}RT_a \ln \left[\frac{P_{\text{out}}}{P_{\text{in}}} \right] = EX_{\text{losses}} \tag{9}$$

In this work, the exergy efficiency of the air heater is calculated based on the exergy losses to expose the significance of each cause of loss on the exergy efficiency. The various causes of exergy losses are listed below [32].

External exergy loss parameters

- (a) Optical exergy losses ($EX_{\text{loss-opt}}$).
- (b) Exergy losses due to heat transfer between SAH components and environment ($EX_{\text{loss,Qloss}}$).

Internal exergy loss parameters or Exergy destruction terms

- (a) Exergy losses due to fluid friction ($EX_{\text{loss,friction}}$).
- (b) Exergy losses due to absorption of solar irradiation by the absorber plate ($EX_{\text{loss,T}_{\text{ap}},T_{\text{sun}}}$).
- (c) Exergy losses due to transfer of heat to working fluid ($EX_{\text{loss,T}_{\text{ap}},T_f}$).

The exergy efficiency of the air heaters are calculated using the equation given below

$$\eta_{\text{ex}} = 1 - \frac{\Sigma EX_{\text{loss}}}{\Sigma EX_{\text{inlet}}} \tag{10}$$

The net rate of exergy supplied at inlet of the solar air heater is given by:

$$\Sigma EX_{\text{inlet}} = IA_c \left[1 - \frac{4}{3} \left(\frac{T_a}{T_{\text{sun}}} \right) + \frac{1}{3} \left(\frac{T_a}{T_{\text{sun}}} \right)^4 \right] \tag{11}$$

The summation of exergy losses is expressed as:

$$\Sigma EX_{\text{loss}} = (EX_{\text{loss,opt}}) + (EX_{\text{loss,Qloss}}) + (EX_{\text{loss,friction}}) + (EX_{T_{\text{ap}},T_{\text{sun}}-\text{loss}}) + (EX_{\text{loss,T}_{\text{ap}},T_f}) \tag{12}$$

The optical loss of the solar air heater is calculated using the relationship shown below:

$$EX_{\text{loss,opt}} = IA_c (1 - \alpha_p \tau_g) \left[1 - \frac{4}{3} \left(\frac{T_a}{T_{\text{sun}}} \right) + \frac{1}{3} \left(\frac{T_a}{T_{\text{sun}}} \right)^4 \right] \tag{13}$$

The exergy losses due to heat transfer between solar air heater components and environment ($EX_{\text{loss,Qloss}}$) is expressed as:

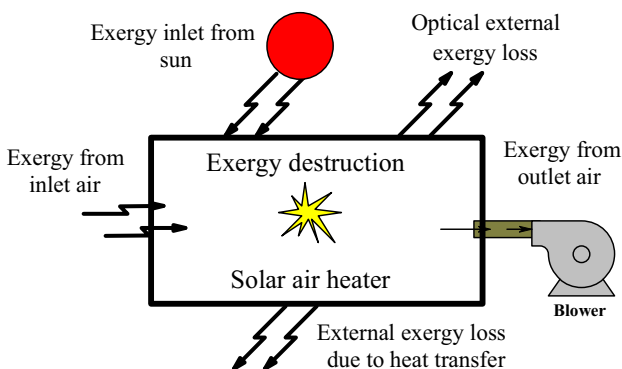


Fig. 2 Exergy balance for SAH

$$EX_{\text{loss}, Q_{\text{loss}}} = U_L A_c (T_{\text{ap}} - T_a) \left[1 - \left(\frac{T_a}{T_{\text{ap}}} \right) \right] \quad (14)$$

where

$$U_L = U_t + U_b \quad (15)$$

In the above equation U_b is known as bottom loss coefficient and U_t indicates top loss coefficient.

The exergy losses due to absorption of solar irradiation by the absorber plate ($EX_{T_{\text{ap}}, T_{\text{sun}} - \text{loss}}$) is given by

$$EX_{T_{\text{ap}}, T_{\text{sun}} - \text{loss}} = I A_c \alpha_p \tau_g \left[1 - \frac{4}{3} \left(\frac{T_a}{T_{\text{sun}}} \right) + \frac{1}{3} \left(\frac{T_a}{T_{\text{sun}}} \right)^4 - \left(1 - \frac{T_a}{T_{\text{ap}}} \right) \right] \quad (16)$$

Finite temperature difference between the absorber plate and fluid causing the exergy destruction is given by:

$$EX_{\text{loss}, T_{\text{ap}}, T_f} = I A_c \eta_{\text{th}} T_a \left[\left(\frac{1}{T_f} \right) - \left(\frac{1}{T_{\text{ap}}} \right) \right] \quad (17)$$

The exergy loss due to fluid friction along the length of air flow path is given by:

$$(EX_{\text{loss}, \text{friction}}) = \frac{T_a \dot{m} \Delta p}{\rho T_f} \quad (18)$$

Analytical model and solution procedure

To evaluate the thermal performance of the multiple arc protrusion roughened plate and smooth plate with jet impingement, SAH uses the identical procedure that was used in artificial roughened plate SAHs [23–26]. During the analysis, the useful heat gain by the absorber plate, energy transferring to the working fluid and heat losses to the environment are calculated by considering the following assumptions: [26, 31]

- (1) The analysis is conducted at steady-state condition with one dimensional heat flow.
- (2) Heat conduction and leakages along the flow direction are negligible.
- (3) Edge effects are negligible.

In this work, the multiple arc shape protrusion roughened plate design parameters are optimized for yielding the maximum exergetic efficiency as a function of Reynolds number (Re) and temperature rise parameter ($\Delta T/I$).

Step 1 The typical values of design configurations and operating conditions of the solar air heater to be analyzed are selected from Table 1.

Step 2 In this analysis, the inlet temperature (T_i) of the SAH is equal to ambient temperature (T_a). Then, the outlet temperature (T_o) of the air heater is calculated using

Table 1 Typical values of operating and design parameters used in analytical study

Parameters	Base values
Design and operating parameters	
Duct length (L)/m	1.1
Duct width (W_p)/m	0.3
Duct depth (Z)/m	0.025
Thickness of insulation (L_i)/m	0.05
Thermal conductivity of insulation (K_i)/W m ⁻¹ K ⁻¹	0.037
Number of glass covers (N)	1
Effective transmittance absorptance product ($\tau\alpha$)	0.85
Emissivity of absorber plate (ϵ_{ap})	0.9
Emissivity of glass cover (ϵ_g)	0.88
Relative width ratio (W_p/W_{AP})	1–5
Relative height ratio (e_p/d_p)	0.5–2
Relative pitch ratio (P_p/e_p)	8–12
Relative angle of arc ($\alpha_a/55$)	35°–75°
Stream wise pitch ratio, X/D	0.433
Span wise pitch ratio, Y/D	0.866
Jet diameter ratio, D_j/D	0.065
Ambient conditions	
Atmospheric temperature (T_a)/K	300
Wind velocity (V_w)/m s ⁻¹	1.5
Sun temperature (T_s)/K	5800
Temperature rise parameter ($\Delta T/I$)/K m ² W ⁻¹	0.007–0.140
Solar intensity (I)/W m ⁻²	700–1000

Eqs. 19 and 20 by considering the desired temperature rise parameter ($\Delta T/I$).

$$T_o = T_i + \Delta T \quad (19)$$

$$\Delta T = \frac{\Delta T}{I} \times I \quad (20)$$

Step 3 Based on the inlet and outlet temperatures, the average fluid temperature (T_f) inside a duct and thermo-physical properties of air such as specific heat (C_p), thermal conductivity (K), dynamic viscosity (μ) are calculated by using empirical correlations proposed by [33] as shown below

$$T_f = \frac{T_o + T_i}{2} \quad (21)$$

$$C_p = 1.0057 + 0.000066(T_f - 27) \quad (22)$$

$$\rho = 1.1774 - 0.00359(T_f - 27) \quad (23)$$

$$K = 0.02624 + 0.0000758(T_f - 27) \quad (24)$$

$$\mu = [1.983 + 0.00184(T_f - 27)] \times 10^{-5} \quad (25)$$

Step 4 The overall heat loss coefficient (U_L) value calculated by summing up of each losses that occurring at top

(U_t), back (U_b) and edge (U_e) loss coefficients can be written as:

$$U_L = U_t + U_b + U_e \tag{26}$$

The back and edge loss coefficients are calculated using Eqs. 27 and 28 as shown below

$$U_b = \frac{K_i}{L_i} \tag{27}$$

$$U_e = \frac{(L + W)ZK_i}{LWL_i} \tag{28}$$

The top loss (U_t) occurred from the solar air heater is calculated using the expression as stated [34].

$$U_t = \left[\frac{N}{\frac{C_t}{T_{ap}} \left(\frac{T_{ap} - T_a}{N + f_t} \right)^{0.33}} + \frac{1}{h_w} \right]^{-1} + \left[\frac{\sigma(T_{ap}^2 + T_a^2)(T_{ap} + T_a)}{\frac{1}{(\epsilon_p + 0.05N(1 - \epsilon_p))} + \frac{2 \times N + f_t - 1}{\epsilon_g}} - 1 \right] \tag{29}$$

where

$$h_w = 5.7 + 3.8V_w,$$

$$C_t = 365.9(1 - 0.00883 \times \beta_t + 0.0001298 \times \beta_t^2)$$

$$f_t = (1 - 0.04 \times h_w + 0.0005 \times h_w^2)(1 + 0.091 \times N)$$

In the above equation, the initial temperature of the absorber plate (T_{AP}) can be approximated as:

$$T_{ap} = \frac{T_i + T_o}{2} + 10^\circ\text{C} \tag{30}$$

Step 5 The rate of useful heat gain (Q_{u1}) collected by the solar air heater is calculated by Eq. 31

$$Q_{u1} = A_c [I(\tau\alpha) - U_L(T_{ap} - T_a)] \tag{31}$$

Step 6 The mass flow rate through the channel (m), mass flux (G) and Reynolds number (Re) of the flow are obtained by the following expressions

$$m = \frac{Q_{u1}}{C_p \Delta T} \tag{32}$$

$$G = \frac{m}{WZ} \tag{33}$$

$$Re = \frac{GD}{\mu} \tag{34}$$

Step 7 The heat transfer coefficient between the absorber plate and impingement air are calculated by first assessing the Nusselt number. The Nusselt number correlation developed based on the experimental results by Nadda et al. [30] is expressed as:

$$\begin{aligned} Nu &= 0.0476Re^{1.0119} \left[\frac{W_A}{W_{AP}} \right]^{0.4228} \\ &\times \exp \left[0.0529 \left(\ln \left(\frac{W_A}{W_{AP}} \right) \right)^2 \right] \left[\frac{e_P}{d_P} \right]^{-0.133} \\ &\times \exp \left[-0.228 \left(\ln \left(\frac{e_P}{d_P} \right) \right)^2 \right] \left[\frac{P_P}{e_P} \right]^{-0.1455} \\ &\times \exp \left[-0.3069 \left(\ln \left(\frac{P_P}{e_P} \right) \right)^2 \right] \left(\frac{\alpha_a}{55} \right)^{-0.7522} \\ &\times \exp \left(-1.4876 \left(\ln \left(\frac{\alpha_a}{55} \right) \right)^2 \right) \end{aligned} \tag{35}$$

Based on the Nusselt number, the heat transfer coefficient is calculated as:

$$h = \frac{Nu K}{D} \tag{36}$$

Step 8 The equations shown in Eqs. 37 and 38 are used to calculate the collector efficiency factor (F_P) and heat removal factor (F_R).

$$F_P = \frac{h}{h + U_L} \tag{37}$$

$$F_R = \frac{mC_p}{U_L A_c} \left[\exp \left(\frac{U_L A_c F_P}{mC_p} \right) - 1 \right] \tag{38}$$

Step 9 Based on the heat removal rate (F_R), the useful energy gained (Q_{u2}) by the air heater is calculated using the expression:

$$Q_{u2} = F_R [I(\tau\alpha) - U_L(T_o - T_i)] A_c \tag{39}$$

Step 10 The useful heat gains Q_{u1} and Q_{u2} are calculated using Eqs. 31 and 39. If the difference between the heat gain values exceeds 0.01%, then the temperature of the absorber plate is recalculated and updated by the expression as:

$$T_{AP} = T_a + \left[\frac{I(\tau\alpha) - Q_{u2}/A_c}{U_L} \right] \tag{40}$$

Then, the iterative process has been continued until the convergence criterion is to be achieved.

Step 11 Then, the thermal efficiency and of the solar air heater is calculated by considering the average values of useful heat gain (Q_{u1} and Q_{u2}) and substituting in Eq. 1.

Step 12 The friction factor calculated by the correlation developed by Nadda et al. [30] based on experimental results can be expressed as:

$$\begin{aligned}
 f = & 15.601 Re^{-0.1434} \left[\frac{W_A}{W_{AP}} \right]^{0.2569} \exp \left[0.1205 \left(\ln \left(\frac{W_A}{W_{AP}} \right) \right)^2 \right] \\
 & \times \left[\frac{e_P}{d_P} \right]^{-0.1708} \exp \left[-0.3957 \left(\ln \left(\frac{e_P}{d_P} \right) \right)^2 \right] \left[\frac{P_P}{e_P} \right]^{-0.2777} \\
 & \times \exp \left[-0.5793 \left(\ln \left(\frac{P_P}{e_P} \right) \right)^2 \right] \left(\frac{\alpha_a}{55} \right)^{-0.9011} \\
 & \times \exp \left(-1.7618 \left(\ln \left(\frac{\alpha_a}{55} \right) \right)^2 \right)
 \end{aligned}
 \tag{41}$$

Step 13 The pressure drop occurred at various flow rate are calculated using the following relationship

$$\Delta P = \frac{4fL\rho V^2}{2D_h}
 \tag{42}$$

Step 14 Further, the thermo-hydraulic and exergetic efficiency of the solar collector can be calculated using the equations from 3 to 18. The iterative procedure, explained

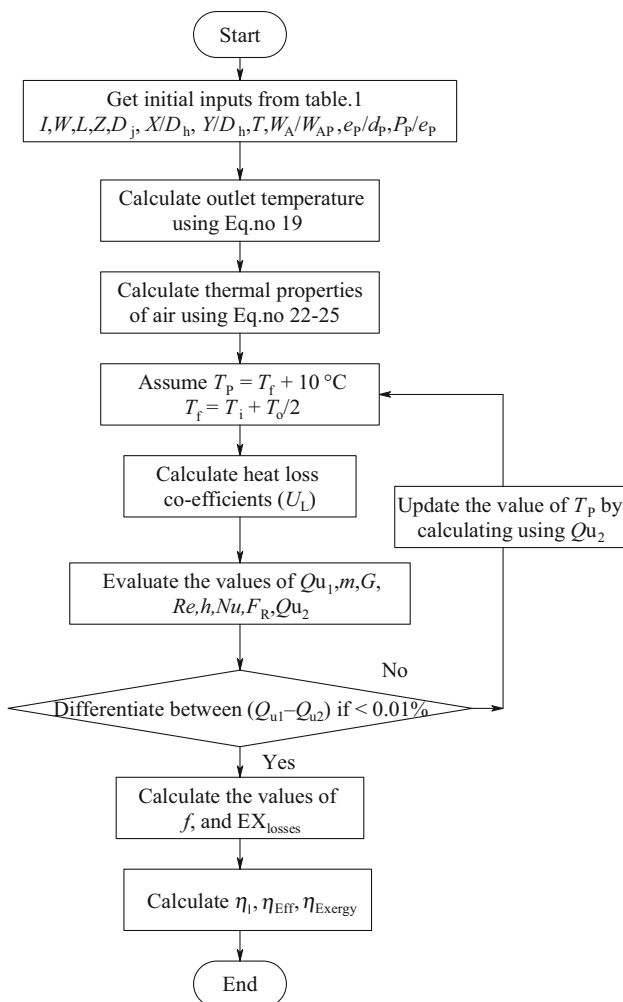


Fig. 3 Flow chart for analytical solution procedure

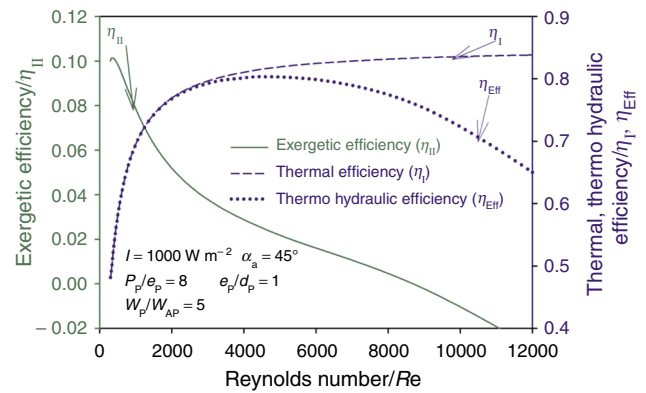


Fig. 4 Variation of thermal, thermo-hydraulic and exergetic efficiency with Reynolds number for SAH with jet impingement on multiple arc-shaped obstacles

in flowchart, shown in Fig. 3 is repeated for the range of design parameters related to absorber plate roughness and temperature rise parameters.

Results and discussions

By considering the entire range of design parameters and operating conditions as given in Table 1, the exergetic efficiency is analytically calculated. Figure 4 shows the thermal, thermo-hydraulic and exergetic efficiency as a function of Reynolds number of a multiple arc shape protrusion roughened jet plate solar air heater for the roughness values of $P_P/e_P = 8$, $\alpha_a = 45^\circ$, $e_P/d_P = 1$, $W_P/W_{AP} = 5$ and solar insolation of 1000 W m^{-2} . It is seen from the figure that the thermal efficiency increases monotonically with increase in Reynolds number. This is due to the fact that increase in Reynolds number results in an increase in impingement air velocity and consequently enhances the heat transfer coefficient and heat capacity of air. The thermo-hydraulic efficiency of SAH is equal to thermal

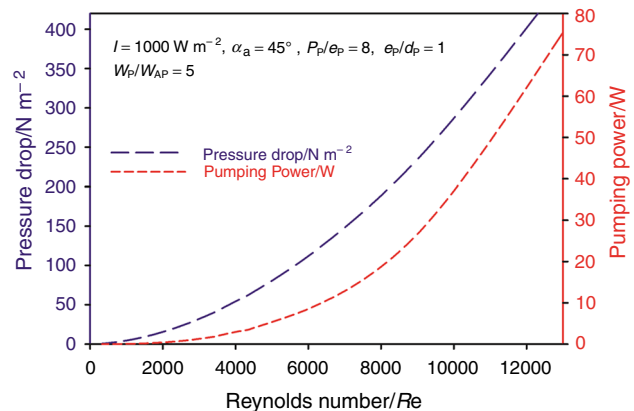


Fig. 5 Variation of pressure drop and pumping power with Reynolds number for jet impingement on multiple arc-shaped obstacles SAH

efficiency up to Re equal to 2300. Further increase in Reynolds number decreases the thermo-hydraulic efficiency. This happens due to fact that when Re increases, the pressure drop and pumping power also increases as shown in Fig. 5. It is also observed from the figure that when $Re > 4200$, there is severe rise in pressure drop and pumping power to overcome the fluid friction and turbulence intensity formed inside the duct.

The exergetic efficiency follows an ascending trend up to Re 400 and yields the maximum exergetic efficiency of 10.1% and starts to falls on descending trend on further increase in Reynolds number. The exergetic performance of the solar air heater has been low in the entire range of Reynolds number and falls into negative region when the $Re \geq 9000$. This happens due to that the various exergy losses, especially exergy required for pumping power to overcome the friction associated with solar air heater duct that outstrips the value of useful thermal exergy collected by solar air heater. The relation between the thermal, thermo-hydraulic and exergy efficiency with the temperature rise parameter ($\Delta T/I$) is shown in Fig. 6. This figure shows that when the temperature rise parameter increases, the exergetic efficiency increases up to the value of $0.135 \text{ K m}^2 \text{ W}^{-1}$ then it starts decreasing. During this condition, the thermal efficiency follows a descending trend with the temperature rise parameter. However, the thermo-hydraulic efficiency is lesser than thermal efficiency up to $\Delta T/I \leq 0.024 \text{ K m}^2 \text{ W}^{-1}$. Further, increase in $\Delta T/I$ deduces the thermo-hydraulic performance and it is equal to thermal efficiency of SAH.

The exergy losses related to global irradiation are shown in Fig. 7. It is observed that about 14.5% of exergy losses occur due to the inefficiency of glass cover and this optical loss ($EX_{\text{loss,Opt}}/EX_{\text{Sun}}$) remains constant and not varies with respect to Reynolds number, absorber plate and fluid temperatures. This happens due to that the effective transmittance absorptance product ($\alpha_p \tau_g$) in Eq. 13 is equal

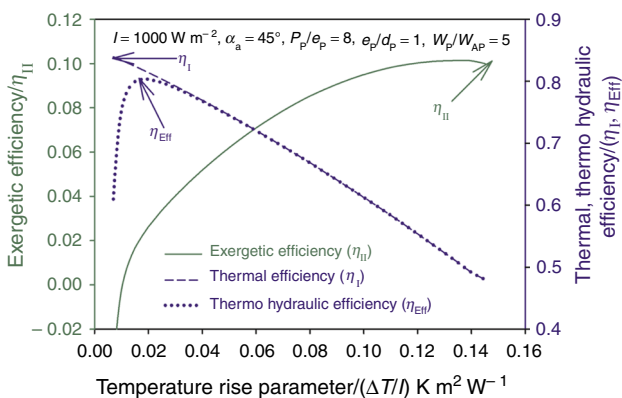


Fig. 6 Variation of thermal thermo-hydraulic and exergetic efficiency with temperature rise parameter with jet impingement on multiple arc-shaped obstacles

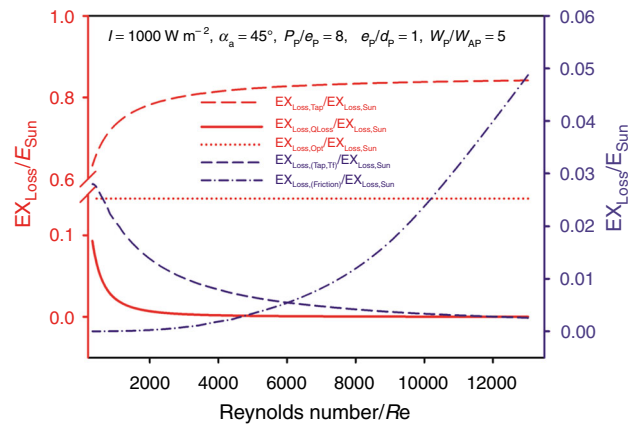


Fig. 7 Various components of exergy losses as a function of Reynolds number for SAH with jet impingement on multiple arc-shaped obstacles

to 0.85. Therefore, the remaining exergy input is continuously loss at all the operating conditions of SAH. The exergy losses occurred between the sun and absorber plate ($EX_{\text{loss,Tap}}/EX_{\text{Sun}}$) is about 63–84%. This is the major source of exergy loss that increases monotonically with Reynolds number. This happens due to that when the air flow rate increases the absorber plate temperature decreases. Consequently, this enhances the exergy destruction in absorber plate and decreases the exergy loss to the environment ($EX_{\text{loss,Qloss}}/EX_{\text{Sun}}$). Thus, at lower mass flow rates, $EX_{\text{loss,Qloss}}/EX_{\text{Sun}}$ is high. The exergy losses associated with internal irreversibilities are due to heat transfer between air and absorber plate due to finite temperature difference, ($EX_{\text{loss,TAP,Tf}}/EX_{\text{Sun}}$), friction along the duct ($EX_{\text{loss,Friction}}/EX_{\text{Sun}}$). The exergy loss $EX_{\text{loss,TAP,Tf}}/EX_{\text{Sun}}$ gradually decreases with Reynolds number due to reduction in temperature difference between inlet and outlet air. The exergy destruction due to friction increases with

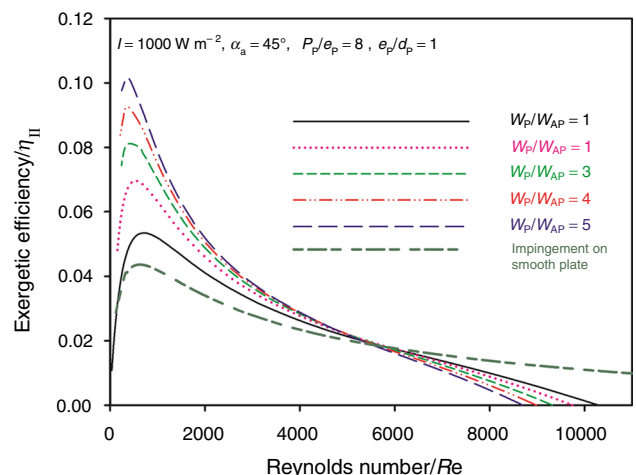


Fig. 8 Exergetic efficiency as function of Reynolds number and relative width ratio (W_A/W_{AP})

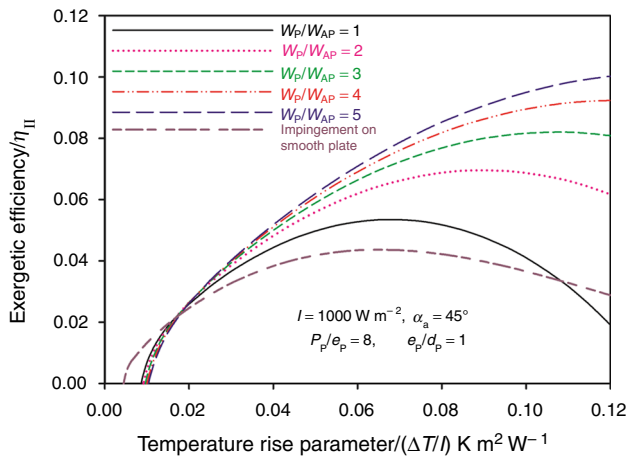


Fig. 9 Exergetic efficiency as function of temperature rise parameter and relative width ratio

increasing in Reynolds number due to higher pumping power and turbulent intensity.

Figures 8 and 9 summarize the effect of relative width ratio (W_p/W_{AP}) based on Reynolds number (Re) and temperature rise parameter ($\Delta T/I$) on the exergetic performance (η_{II}) of the solar air heater for solar insolation of 1000 W m^{-2} , while other roughness parameters are constant. From Fig. 8, it is observed that the relative width ratio (W_p/W_{AP}) of 5 yields the maximum exergetic efficiency (η_{II}) for $Re < 4800$, and for $Re > 5900$, the smooth plate with jet impingement SAH yields the maximum exergetic efficiency (η_{II}). When the Re is in the range of 4800–5900, the highest exergetic efficiency occurs for various values of W_p/W_{AP} in the range of 1–4. This happens due to increase in width ratio leads to formation of leading ends and secondary flow cells. It can be seen from Fig. 9 that the smooth plate with jet

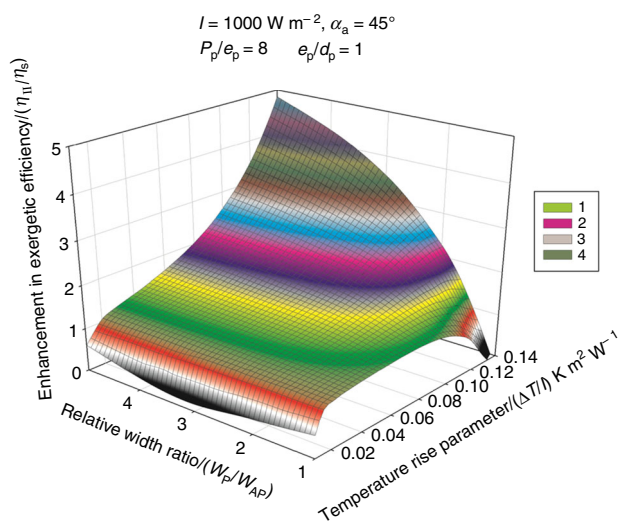


Fig. 10 Enhancement in exergetic efficiency as function of temperature rise parameter and relative width ratio (W_A/W_{AP})

impingement SAH performs better by producing higher exergetic efficiency compared with multiple arc shape protrusion roughened plate with jet impingement SAH for $\Delta T/I < 0.015 \text{ K m}^2 \text{ W}^{-1}$. For $\Delta T/I > 0.033 \text{ K m}^2 \text{ W}^{-1}$, the maximum value of exergetic efficiency is obtained for the relative width ratio (W_p/W_{AP}) equal to 5. When the $\Delta T/I$ is in the range of $0.015\text{--}0.033 \text{ K m}^2 \text{ W}^{-1}$, the highest exergetic efficiency occurs for various values of W_p/W_{AP} in the range of 1–4. Figure 10 shows the enhancement in exergetic efficiency (η_{II}/η_s) as a function of temperature rise parameter for various values of relative width ratio (W_p/W_{AP}). The maximum enhancement has been found at for $W_p/W_{AP} = 5$ except at low values of $\Delta T/I$. The rate of enhancement is high when the W_p/W_{AP} is increased from 1 to 2 as it compared with further increment in the values of W_p/W_{AP} .

For constant roughness parameters, Figs. 11 and 12 summarize the effect of relative height ratio (e_p/d_p) based on Reynolds number (Re) and temperature rise parameter ($\Delta T/I$) on the exergetic performance (η_{II}) of the solar air heater for solar insolation of 1000 W m^{-2} . From Fig. 11, it is observed that the relative height ratio (e_p/d_p) of 1 yields the maximum exergetic efficiency (η_{II}) for $Re < 4100$, and for $Re > 5900$, the smooth plate with jet impingement SAH yields the maximum exergetic efficiency (η_{II}). When relative height ratio increases, the reattachment vicinity is more in the range of 0.5–1. The further increment in height ratio leads to reduction in exergetic efficiency due to less reattachment vicinity. When the Re is in the range of 4100–5900, the highest exergetic efficiency occurs for various values of e_p/d_p in the range of 0.5–2 due to better movement of resulting vortices. It can be seen from Fig. 12 that the smooth plate with jet impingement SAH performs better when the $\Delta T/I < 0.015 \text{ K m}^2 \text{ W}^{-1}$ and for $\Delta T/I > 0.022 \text{ K m}^2 \text{ W}^{-1}$, the maximum value of exergetic efficiency is obtained for e_p/d_p equal to 1. When the $\Delta T/I$ is

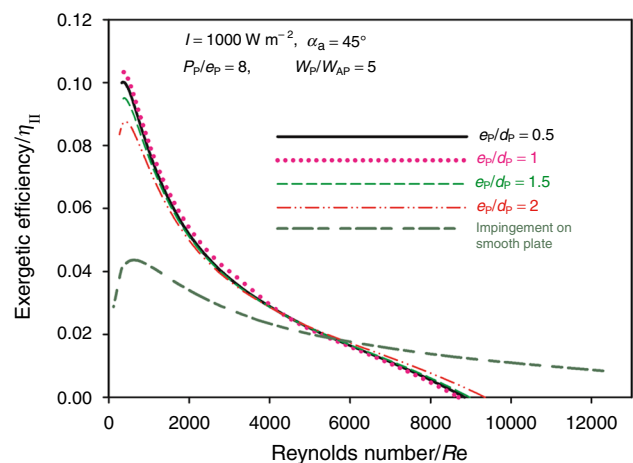


Fig. 11 Exergetic efficiency as function of Reynolds number and relative height ratio (e_p/d_p)

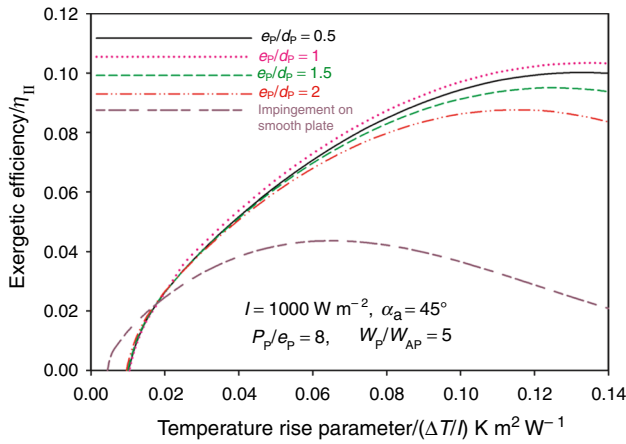


Fig. 12 Exergetic efficiency as function of temperature rise parameter and relative height ratio (e_p/d_p)

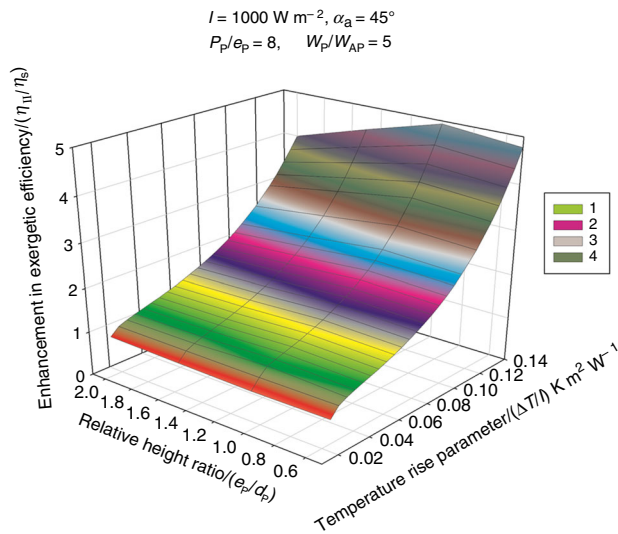


Fig. 13 Enhancement in exergetic efficiency as function of temperature rise parameter and relative height ratio (e_p/d_p)

in the range of 0.015–0.022 $K m^2 W^{-1}$, the highest exergetic efficiency is observed for various values of e_p/d_p in the range of 0.5–2. Figure 13 reveals the enhancement in exergetic efficiency (η_{II}/η_S) as a function of temperature rise parameter for various values of relative height ratio (e_p/d_p). The maximum enhancement has been found at $e_p/d_p = 1$ except at low values of $\Delta T/I$. The rate of enhancement is high when the e_p/d_p is increased from 0.5 to 1 and further increment in relative height ratio (e_p/d_p) leads to considerable decrement on enhancement.

The variation of exergetic efficiency based on Reynolds number (Re) and temperature rise parameter ($\Delta T/I$) at different values of relative pitch ratio (P_p/e_p) and for solar insolation of $1000 W m^{-2}$, relative height ratio (e_p/d_p) of 1, relative width ratio (W_p/W_{AP}) of 5 and relative angle of arc (α_a) of 45° are shown in Figs. 14 and 15. From Fig. 14,

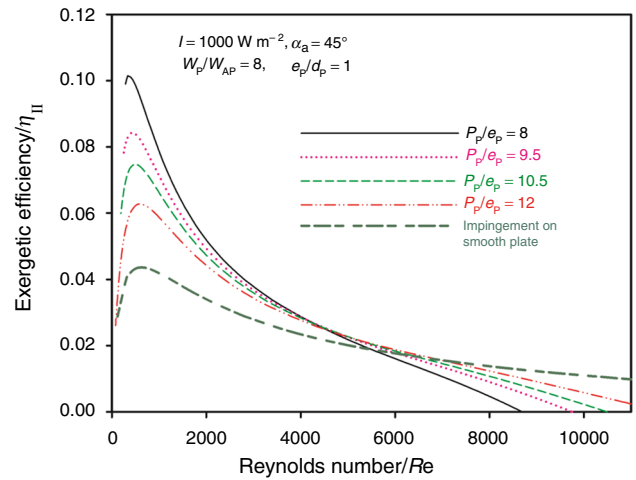


Fig. 14 Exergetic efficiency as function of Reynolds number and relative pitch ratio (P_p/e_p)

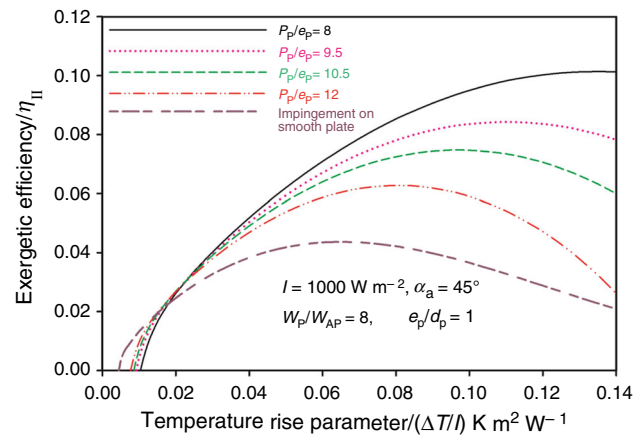


Fig. 15 Exergetic efficiency as function of temperature rise parameter and relative pitch ratio (P_p/e_p)

it is observed that the relative pitch ratio (P_p/e_p) of 8 yields the maximum exergetic efficiency (η_{II}) for $Re < 4000$, and for $Re > 6800$, the smooth plate with jet impingement SAH yields the maximum exergetic efficiency (η_{II}). This happens due to the fact that the flow separation taking place in the downstream of arc-shaped dimple is effectively reattached. When the Re is in the range of 4000–6800, the highest exergetic efficiency occurs for various values of P_p/e_p in the range of 9.5–12 due to better reattachment vicinity. It can be seen from Fig. 15 that the smooth plate with jet impingement SAH performs better when the $\Delta T/I < 0.015 K m^2 W^{-1}$ and for $\Delta T/I > 0.024 K m^2 W^{-1}$, the maximum value of exergetic efficiency is obtained for the relative pitch ratio (P_p/e_p) equal to 8. When the $\Delta T/I$ is in the range of 0.015–0.024 $K m^2 W^{-1}$, the highest exergetic efficiency is observed for various values of P_p/e_p in the range of 9.5–12. Figure 16 reveals the enhancement in exergetic efficiency (η_{II}/η_S) as a function of temperature

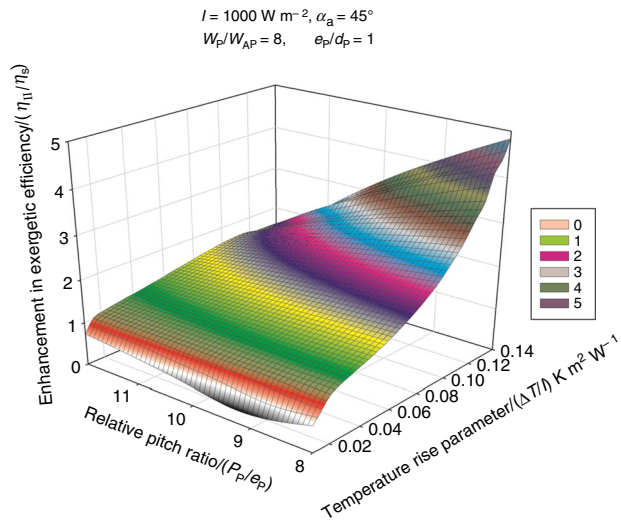


Fig. 16 Enhancement in exergetic efficiency as function of temperature rise parameter and relative pitch ratio (P_p/e_p)

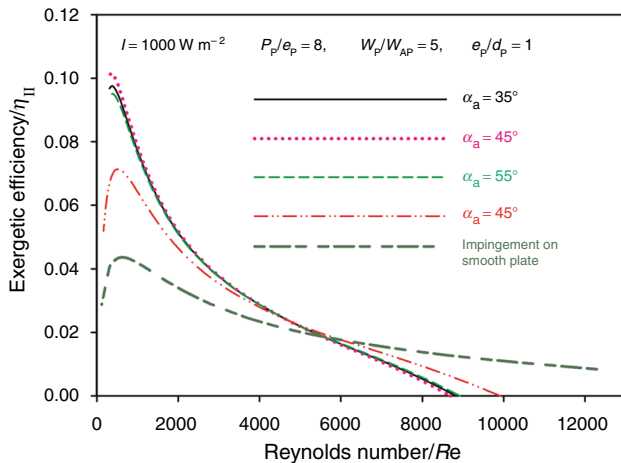


Fig. 17 Exergetic efficiency as function of Reynolds number and angle of arc (α_a)

rise parameter for various values of relative pitch ratio (P_p/e_p). The maximum enhancement is found for $P_p/e_p = 8$ except at low values of $\Delta T/I$ and further increment in relative pitch ratio (e_p/d_p) causes decrement in enhancement ratio.

The variation of exergetic efficiency based on Reynolds number (Re) and temperature rise parameter ($\Delta T/I$) at different relative angle of arc (α_a) and for solar insolation of 1000 W m^{-2} , relative height ratio (e_p/d_p) of 1, relative width ratio (W_p/W_{AP}) of 5 and relative pitch ratio (P_p/e_p) of 8 are shown in Figs. 17 and 18. From Fig. 17, it is observed that the relative angle of arc (α_a) of 45° yields the maximum exergetic efficiency (η_{II}) for $Re < 4400$ and for $Re > 6100$, the smooth plate with jet impingement SAH yields the maximum exergetic efficiency (η_{II}). This is due

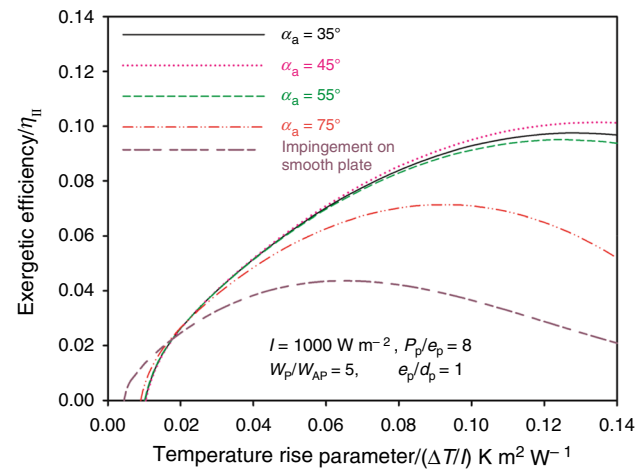


Fig. 18 Exergetic efficiency as function of temperature rise parameter and angle of arc (α_a)

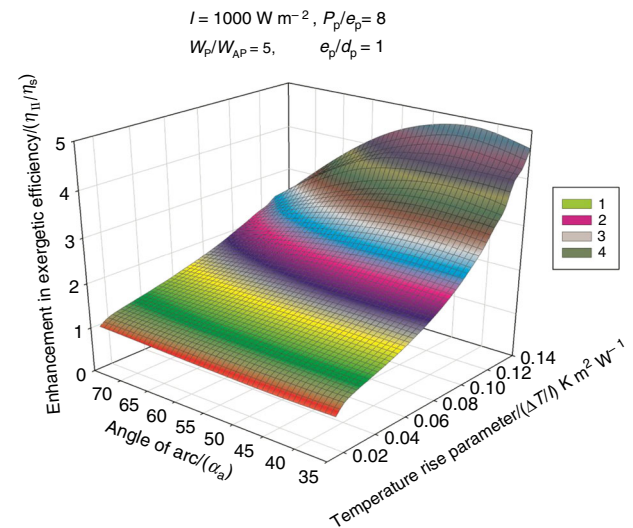


Fig. 19 Enhancement in exergetic efficiency as function of temperature rise parameter and angle of arc (α_a)

to the fact that the flow separation, by leading edges induces more vortices.

When the Re is in the range of 4400–6100, the highest exergetic efficiency occurs for various values of α_a in the range of 35° – 75° . It can be seen from Fig. 18 that the smooth plate with jet impingement SAH performs better when the $\Delta T/I < 0.016 \text{ K m}^2 \text{ W}^{-1}$ and for $\Delta T/I > 0.03 \text{ K m}^2 \text{ W}^{-1}$, the maximum value of exergetic efficiency is obtained for the relative angle of arc (α_a) equal to 45° . When the $\Delta T/I$ is in the range of 0.016 – $0.03 \text{ K m}^2 \text{ W}^{-1}$, the highest exergetic efficiency is observed for various values of α_a in the range of 35° – 75° . For various values of relative angle of arc (α_a), Fig. 19 reveals enhancement in exergetic efficiency (η_{II}/η_S) as a function of temperature rise parameter. The maximum

enhancement is found for $\alpha_a = 45^\circ$ except at low values of $\Delta T/I$. The rate of enhancement is high when the α is increased from 35° to 45° and further increment in relative angle of arc (α_a) leads to considerable decrement on enhancement ratio.

From the above discussions, it is observed that there are no particular set of geometrical roughness parameter yielding the maximum exergetic efficiency (η_{II}) for the entire range of Reynolds number and temperature rise parameter ($\Delta T/I$). It can be observed from Figs. 8, 11, 14, and 17 that the exergetic efficiency follows an increasing trend with Reynolds number and reaches the maxima value; then, it follows a diminishing trend. This happens due to the fact that pumping power dominates the useful heat gain at higher values of Reynolds number. From the figures, it is also seen that the multiple arc shape protrusion roughened plate with jet impingement SAH can be effectively operated for Reynolds number in the range of 400–5900 for obtaining the highest exergetic efficiency. Figures 10, 13, 16 and 19 show that the maximum enhancement in exergetic efficiency ratio is 4.84, corresponding to geometrical roughness parameter values of $W_p/W_{AP} = 5$, $e_p/d_p = 1$, $P_p/e_p = 8$, $\alpha_a = 45^\circ$.

The exergetic performance for multiple arc protrusion roughened SAH with jet impingement is compared with discrete V-down rib roughness shape [23] and protruded arc shape roughened geometry [24] under identical operating conditions are shown in Fig. 20. From this figure, it is concluded that multiple arc protrusion roughened SAH with jet impingement has better performance when the $Re < 4200$. From this figure, it is also observed that when Re increases, there is a significant drop in exergetic efficiency. This is due to fact that there is sudden increment in pressure drop and pumping power consumption as observed from Fig. 5. And also, from Fig. 7, it is observed that increase in pressure drop improves the exergy

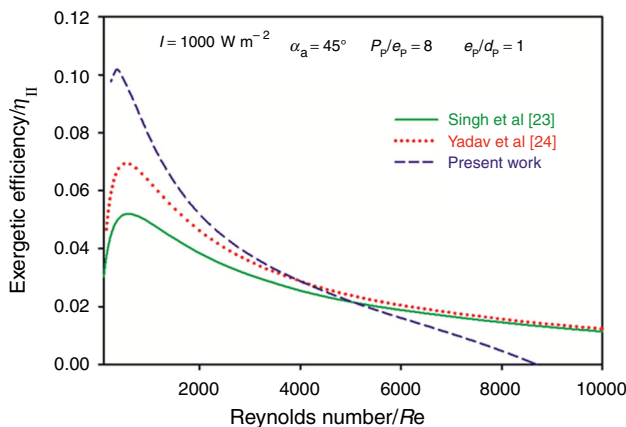


Fig. 20 Comparison of exergetic efficiency values for protrusions with other SAH in literature

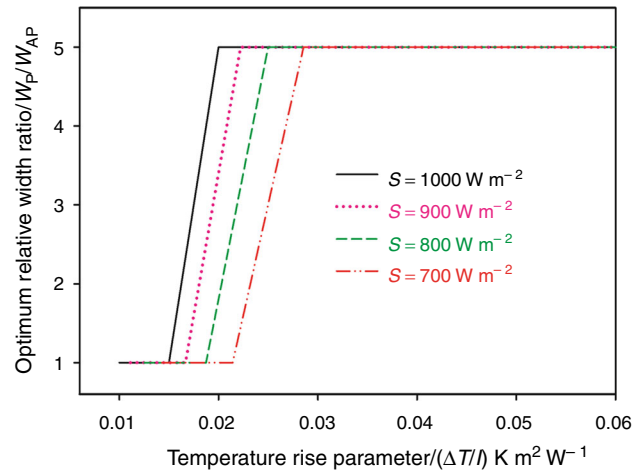


Fig. 21 Optimum values of relative width ratio (W_p/W_{AP}) on the basis of maximum exergetic efficiency criterion

destruction ($EX_{loss,Friction}/EX_{Sun}$) due to friction from 1 to 5%. This also results in degrading the exergetic performance of SAH.

Design plots for optimum multiple arc protrusion roughness parameters

The highest values of exergetic efficiency yielded by the multiple arc shape protrusion roughened SAH parameters such as relative width ratio (W_p/W_{AP}), relative height ratio (e_p/d_p), relative pitch ratio (P_p/e_p) and relative angle of arc (α_a) for different temperature rise parameters are shown in Figs. 21–24, respectively. It can be observed from Fig. 21 that for all the values of solar radiation, the relative width ratio (W_p/W_{AP}) of 5 is optimum for $\Delta T/I > 0.0286 \text{ K m}^2 \text{ W}^{-1}$ and relative width ratio (W_p/W_{AP}) of 1 is optimum for $\Delta T/I < 0.015 \text{ K m}^2 \text{ W}^{-1}$. When the $\Delta T/I$ is in the range of $0.015\text{--}0.0286 \text{ K m}^2 \text{ W}^{-1}$, the

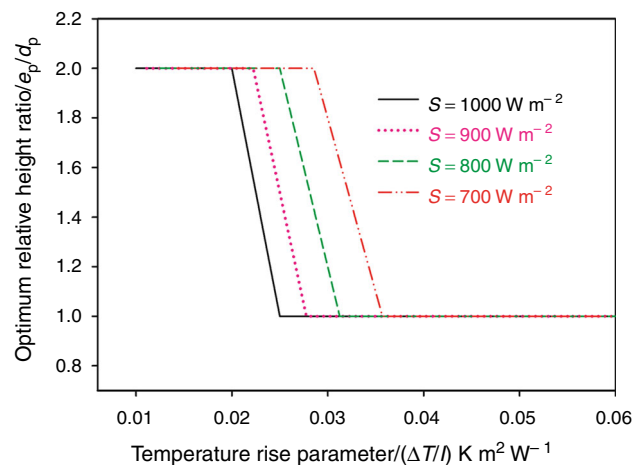


Fig. 22 Optimum values of relative height ratio (e_p/d_p) on the basis of maximum exergetic efficiency criterion

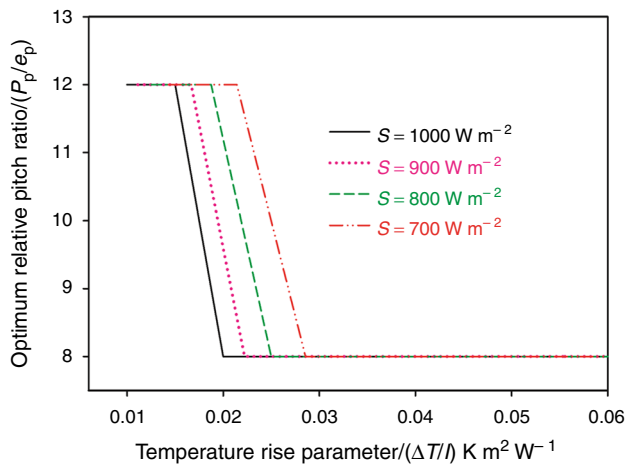


Fig. 23 Optimum values of relative pitch ratio (P_p/e_p) on the basis of maximum exergetic efficiency criterion

optimum values depends on solar insolation and temperature rise parameter. Figure 22 shows that the relative height ratio (e_p/d_p) of 1 is optimum for $\Delta T/I > 0.035 \text{ K m}^2 \text{ W}^{-1}$ and relative height ratio (e_p/d_p) of 2 is optimum for $\Delta T/I < 0.019 \text{ K m}^2 \text{ W}^{-1}$ for all the values of solar radiation. When the $\Delta T/I$ is in the range of $0.019\text{--}0.035 \text{ K m}^2 \text{ W}^{-1}$, the optimum values depend on solar insolation and temperature rise parameter. For all the values of solar radiation, Fig. 23 shows that the relative pitch ratio (P_p/e_p) of 8 is optimum for $\Delta T/I > 0.028 \text{ K m}^2 \text{ W}^{-1}$ and relative pitch ratio (P_p/e_p) of 12 is optimum for $\Delta T/I < 0.015 \text{ K m}^2 \text{ W}^{-1}$. When the $\Delta T/I$ is in the range of $0.015\text{--}0.028 \text{ K m}^2 \text{ W}^{-1}$, the optimum values depend on solar insolation and temperature rise parameter. For all the values of solar radiation, Fig. 24 reveals that the relative angle of arc (α_a) of 45° is optimum for $\Delta T/I > 0.035 \text{ K m}^2 \text{ W}^{-1}$ and relative angle of arc (α_a) of 75° is optimum for $\Delta T/I < 0.02 \text{ K m}^2 \text{ W}^{-1}$. When the $\Delta T/I$ is

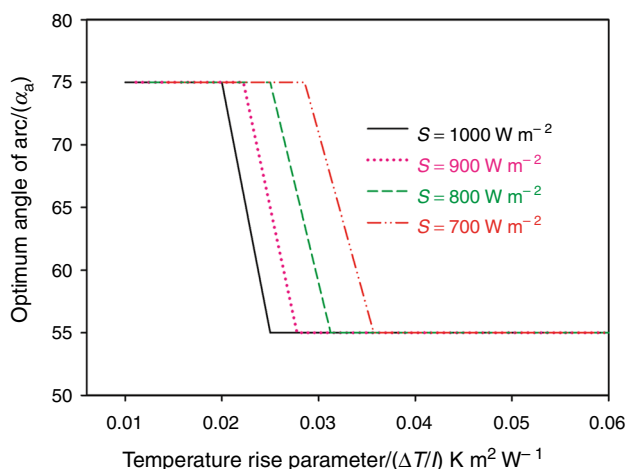


Fig. 24 Optimum values of angle of arc (α_a) on the basis of maximum exergetic efficiency criterion

in the range of $0.02\text{--}0.035 \text{ K m}^2 \text{ W}^{-1}$, the optimum values depend on solar insolation and temperature rise parameter.

Conclusions

In this present work, a mathematical model has been developed for predicting the exergetic efficiency of a multiple arc shape protrusion roughened plate with jet impingement solar air heater. The influence of Reynolds number and roughness parameters on exergetic efficiency has been determined. The performance of multiple arc shape protrusion roughened plate with jet impingement SAH has been compared with smooth plate with jet impingement SAH at analogous conditions and following conclusions have been attained.

- The multiple arc shape protrusion roughened plate with jet impingement SAH performs better up to the Reynolds number equal to 5900 and above this value smooth plate with jet impingement SAH is appropriate.
- The maximum exergetic efficiency of multiple arc shape protrusion roughened plate with jet impingement SAH is 10.5%. By using this configuration of solar air heater, the exergetic efficiency is improved up to 56.8% as compared with smooth plate jet impingement SAH.
- The optimum values of roughness parameters that yields the maximum exergetic efficiency for the Re ranges from 400 to 5900 are relative width ratio (W_p/W_{AP}) of 5, relative height ratio (e_p/d_p) of 1, relative pitch ratio (P_p/e_p) of 8 and relative angle of arc (α_a) of 45°
- For each roughness parameters of absorber plate, a separate design plots are prepared as a function of temperature rise parameter which are used to assess the system performance at different operating conditions to yield the maximum exergetic efficiency.

References

1. Bansal NK. Solar air heater applications in India. *Renew Energy*. 1999;16:618–23.
2. Sharma SK, Kalamkar VR. Thermo-hydraulic performance analysis of solar air heaters having artificial roughness—a review. *Renew Sustain Energy Rev*. 2015;41:413–35.
3. Malliga TV, Rajasekhar RJ. Preparation and characterization of nanographite-and CuO based absorber and performance evaluation of solar air-heating collector. *J Therm Anal Calorim*. 2017;129(1):233–40.
4. Stalin PMJ, Arjunan TV, Matheswaran MM, Sadanandam N. Experimental and theoretical investigation on the effects of lower concentration CeO_2 /water nanofluid in flat-plate solar collector. *J Therm Anal Calorim*. 2017. <https://doi.org/10.1007/s10973-017-6865-4>.

5. Kumar A, Saini RP, Saini JS. A review of thermo hydraulic performance of artificially roughened solar air heaters. *Renew Sustain Energy Rev.* 2014;37:100–22.
6. Alam T, Kim MH. Performance improvement of double-pass solar air heater—a state of art of review. *Renew Sustain Energy Rev.* 2017;79:779–93.
7. Kabeel AE, Hamed MH, Omara ZM, Kandael AW. Solar air heaters: design configurations, improvement methods and applications—a detailed review. *Renew Sustain Energy Rev.* 2016;70:1189–206.
8. Choudhury C, Garg HP. Evaluation of a jet plate solar air heater. *Sol Energy.* 1991;46(4):199–209.
9. Belusko M, Saman W, Bruno F. Performance of jet impingement in unglazed air collectors. *Sol Energy.* 2008;82(5):389–98.
10. Chauhan R, Thakur NS. Heat transfer and friction factor correlations for impinging jet solar air heater. *Exp Therm Fluid Sci.* 2013;44:760–7.
11. Chauhan R, Thakur NS. Investigation of the thermo hydraulic performance of impinging jet solar air heater. *Energy.* 2014;68:255–61.
12. Nayak RK, Singh SN. Effect of geometrical aspects on the performance of jet plate solar air heater. *Sol Energy.* 2016;137:434–40.
13. Soni A, Singh SN. Experimental analysis of geometrical parameters on the performance of an inline jet plate solar air heater. *Sol Energy.* 2017;148:149–56.
14. Matheswaran MM, Arjunan TV, Somasundaram D. Energetic, exergetic and enviro-economic analysis of parallel pass jet plate solar air heater with artificial roughness. *J Therm Anal Calorim.* 2018. <https://doi.org/10.1007/s10973-018-7727-4>.
15. Zukowski M. Experimental investigations of thermal and flow characteristics of a novel micro jet air solar heater. *Appl Energy.* 2015;142:10–20.
16. Chauhan R, Singh T, Thakur NS, Patnaik A. Optimization of parameters in solar thermal collector provided with impinging air jets based upon preference selection index method. *Renew Energy.* 2016;99:118–26.
17. Chauhan R, Singh T, Kumar N, Patnaik A, Thakur NS. Experimental investigation and optimization of impinging jet solar thermal collector by Taguchi method. *Appl Therm Eng.* 2017;116:100–9.
18. Brideau SA, Collins MR. Development and validation of a hybrid PV/Thermal air based collector model with impinging jets. *Sol Energy.* 2014;102:234–46.
19. Kumar RA, Babu BG, Mohanraj M. Thermodynamic performance of forced convection solar air heaters using pin–fin absorber plate packed with latent heat storage materials. *J Therm Anal Calorim.* 2016;126(3):1657–78.
20. Mortazavi A, Ameri M. Conventional and advanced exergy analysis of solar flat plate air collectors. *Energy.* 2018;142:277–88.
21. Raj AK, Kunal G, Srinivas MS, Jayaraj S. Performance analysis of a double-pass solar air heater system with asymmetric channel flow passages. *J Therm Anal Calorim.* 2018. <https://doi.org/10.1007/s10973-018-7762-1>.
22. Gupta MK, Kaushik SC. Performance evaluation of solar air heater for various artificial roughness geometries based on energy, effective and exergy efficiencies. *Renew Energy.* 2009;34(3):465–76.
23. Singh S, Chander S, Saini JS. Exergy based analysis of solar air heater having discrete V-down rib roughness on absorber plate. *Energy.* 2012;37(1):749–58.
24. Yadav S, Kaushal M. Exergetic performance evaluation of solar air heater having arc shape oriented protrusions as roughness element. *Sol Energy.* 2014;105:181–9.
25. Sahu MK, Prasad RK. Exergy based performance evaluation of solar air heater with arc-shaped wire roughened absorber plate. *Renew Energy.* 2016;96:233–43.
26. Chamoli S, Thakur NS. Exergetic performance evaluation of solar air heater having V-down perforated baffles on the absorber plate. *J Therm Anal Calorim.* 2014;117(2):909–23.
27. Bahremand D, Ameri M, Gholampour M. Energy and exergy analysis of different solar air collector systems with forced convection. *Renew Energy.* 2015;83:1119–30.
28. Hedayatizadeh M, Ajabshirchi Y, Sarhaddi F, Farahat S, Safavinejad A, Chaji H. Analysis of exergy and parametric study of a v-corrugated solar air heater. *Heat Mass Transf.* 2012;48(7):1089–101.
29. Hedayatizadeh M, Sarhaddi F, Safavinejad A, Ranjbar F, Chaji H. Exergy loss-based efficiency optimization of a double-pass/glazed v-corrugated plate solar air heater. *Energy.* 2016;94:799–810.
30. Nadda R, Kumar A, Maithani R. Developing heat transfer and friction loss in an impingement jets solar air heater with multiple arc protrusion obstacles. *Sol Energy.* 2017;158:117–31.
31. Duffie JA, Beckman WA. *Solar engineering thermal processes.* New York: Wiley; 1992.
32. Matheswaran MM, Arjunan TV, Somasundaram D. Analytical investigation of solar air heater with jet impingement using energy and exergy analysis. *Sol Energy.* 2018;161:25–37.
33. Ong KS. Thermal performance of solar air heaters: mathematical model and solution procedure. *Sol Energy.* 1995;55(2):93–109.
34. Klein SA. Calculation of the flat plate collector loss coefficients. *Sol Energy.* 1975;17:79–80.